Original Research

Retinal Features in Cynomolgus Macaques (*Macaca fascicularis*) Assessed by Using Scanning Laser Ophthalmoscopy and Spectral Domain Optical Coherence Tomography

Nora Denk,[1,*] Peter M Maloca,[2-4] Guido Steiner,[1] Helen Booler,[5] Christian Freichel,[1] Stephanie Niklaus,[1] Tobias K Schnitzer,[1] and Pascal W Hasler[4]

Cynomolgus macaques are an important and commonly used species in preclinical toxicology studies, but structural reports of in vivo retinal findings are rare in this species. The purpose of this study was to diminish this gap and document optical coherence tomography and scanning laser ophthalmoscopy imaging data in the healthy posterior pole of cynomolgus monkeys' eyes at predose examinations. The current study is a retrospective assessment of baseline spectral domain OCT data obtained from the 768 eyes of 384 cynomolgus monkeys (192 males and 192 females) of Mauritian origin. The data set was obtained from studies conducted over a 4-y period in the context of ocular safety evaluations of various compounds under preclinical development. The most prevalent findings were the presence of Bergmeister papilla and intravitreal hyperreflective spots. Less common findings included disorganization of retinal zones, abnormalities of the retinal vasculature, partial posterior vitreous detachment, and abnormally shaped foveal pits. Thoughtful consideration of these physiologic findings will aid in distinguishing normal features from toxic outcomes in future preclinical ophthalmic studies.

Abbreviations: HRS, hyperreflective spots; OCT, optical coherence tomography; SD-OCT, spectral-domain optical coherence tomography; SLO, scanning laser ophthalmoscopy

Optical coherence tomography (OCT) has proven to be an extremely valuable diagnostic tool in ophthalmology and has become one of the most frequently used imaging modalities in humans.[8] OCT is a noninvasive imaging technique[11] that provides high-resolution images of various ocular structures in vivo. In contrast to all other fundus-imaging techniques used, OCT enables for high spatial-resolution image display.[27] In recent years, the technique has gained increasing importance in preclinical toxicity studies as it provides a real-time cross-sectional image of ocular structures, most commonly used for imaging of the retina[2] and the optic nerve. Differentiation of individual retinal layers over time facilitates quantitative and repeated noninvasive evaluation during the study time course. Two main variations of OCT have been developed: spectral-domain OCT (SD-OCT) and swept-source OCT. The difference in these 2 modalities lies in the mechanism used to measure interference corresponding to different frequencies. SD-OCT is most commonly used in current preclinical settings.

Cynomolgus macaques are a nonrodent species frequently used in toxicology studies for the safety assessment of pharmaceuticals. Given the similarities in ocular anatomy and physiology between these animals and humans,[1] an appropriate alternative species may not be available for this purpose. OCT examination of cynomolgus macaques is currently commonly used in preclinical toxicology studies and the technique has an important translational contribution, given its routine use in clinical settings.[13] However, no clear standards regarding the imaging technique, nomenclature, or interpretation exist in the preclinical setting, causing a substantial variability when comparing assessments by different testing facilities. In addition, interpretation of OCT scans from studies can be constrained by considerable variability among different animals[4] as well as group size limitations due to animal welfare considerations, logistical feasibility, and expense. Because OCT has been available for a relatively brief time compared with other ophthalmic examination techniques, historical control data are sparse to nonexistent, thus further complicating the interpretation of changes in light of the small sample size in any single study. In addition, marked differences in the description of findings from reviewers in different testing facilities regarding nomenclature and recording threshold for individual findings were considerable. This caveat holds especially true for subtle changes or rather uncommon findings. Therefore, our current study adds new evidence and characterizes the background

retinal findings that can be observed on OCT in untreated cynomolgus monkeys.

Materials and Methods

Animals and husbandry. The review and assessment of data in this study were accomplished through retrospective analysis of raw data from studies conducted in the routine support of pharmaceutical product development. Therefore, no additional animals were used to acquire these data. The study plan and any amendments or procedures involving the care and use of animals in these primary studies had been reviewed and approved by the IACUC of the respective institutions. During the studies, the care and use of animals were conducted according to the guidelines of the US National Research Council or the Canadian Council on Animal Care.

The study population comprised 192 female and 192 male cynomolgus macaques (*Macaca fascicularis*; age, 30 to 50 mo; weight, 2.5 to 5.5 kg) of Mauritian background. The animals were group-housed in stainless steel cages according to European housing standards described in Annex III of Directive 2010/63/EU. The temperature of the animal room was kept between 20 °C and 26 °C, with humidity between 30% and 70% and a 12:12-h light:dark cycle. Animals were fed a standard diet of pellets supplemented with fresh fruits and vegetables. Municipal tap water treated by reverse osmosis and UV irradiation was freely available to each animal via an automated watering system. Psychologic and environmental enrichment was provided to animals except during study procedures and activities.

OCT imaging and evaluation. Scanning laser ophthalmoscopy (SLO) was performed simultaneously with SD-OCT by using the Spectralis HRA +OCT Heidelberg platform (Heidelberg Engineering, Heidelberg, Germany). For some animals, additional red-free or autofluorescence fundus images were obtained depending on the study protocol. The OCT volume scans were performed through the dilated pupil (tropicamide) on cubes with 25 to 31 raster lines, separated by 11 to 218 μm, respectively, depending on the study protocol. The high-resolution scan setting was applied, and OCT images were averaged for 10 to 30 scans by using the automatic averaging and tracking feature. Additional single high-resolution B scans (each averaged with 100 images) were obtained in some studies. Imaging of the animals was performed under general anesthesia (ketamine, 10 mg/kg IM; dexmedetomidine, 25 μg/kg IM) to minimize stress for the animals and ensure a stable eye position. Immediately before the start of OCT imaging, a single dose of midazolam (0.2 mg/kg IM) was administered to keep the eyes centrally positioned.

For the conduct of this study, all original OCT scans were requested and individually reviewed retrospectively. The manufacturer's built-in measurement tool was used to measure the size of selected structures. Image analysis was performed by 2 independent readers (ND, PWH). The Spectralis system measures a signal-to-noise ratio (SNR) in decibels. B-scans with an SNR ratio lower than 25 dB were excluded from the analyse. In addition, concurrent data of slit-lamp examination and indirect ophthalmoscopy were available for review and comparison for each animal.

Statistics. Incidence of findings was reported on an animal level as well as on the level of examined eyes. Numbers were given as either case counts or incidences (in percentage); 95% binomial confidence intervals (Clopper–Pearson method) around the observed incidence rates are reported. For the comparison of incidences in various subgroups, the odds ratio was evaluated by using conditional likelihood estimation with confidence
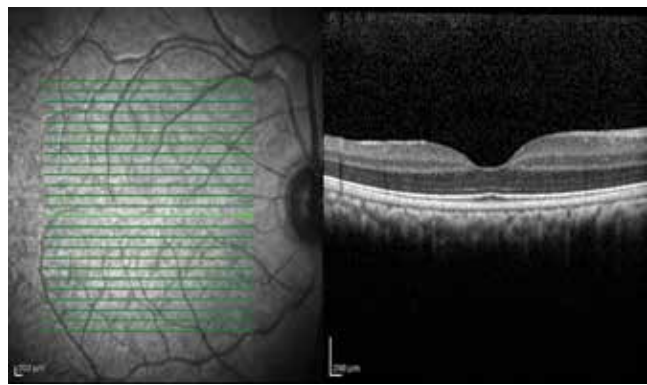

Figure 1. Scanning-laser ophthalmoscopy fundus image of a cynomolgous monkey (left) and the corresponding OCT scan of a healthy macula (right).

interval and *P* value calculated by the Fisher exact method. A *P* value of < 0.05 was considered significant.

Results

This study examined 384 cynomolgus monkeys of Mauritian origin (192 females and 192 males). They contributed 27,604 scans. Representative images of SLO and OCT scans are displayed in Figure 1, and findings are summarized in Table 1.

The most prevalent findings were the presence of elongated remnants of the hyaloid artery (Bergmeister papilla) and intravitreal hyperreflective spots (HRS). Less common findings included discontinuation or disorganization of retinal layers, abnormalities of the retinal vasculature due to increased tortuosity of the retinal vessels, posterior vitreous detachment, and unusually shaped foveal pits.

Bergmeister papilla. Posterior remnants of the hyaloid artery (Bergmeister papilla) was the most common finding. This finding occurred in 198 of the 464 eyes (42.7%) in scans that included the optic disc (Figure 2), and 79% of the animals whose scans included the optic disc showed this finding on at least one eye. The adjacent posterior vitreous displayed a conical reflective structure extending anteriorly from the nasal portion of the optic disc (Figure 2). Males were affected in a significantly higher proportion of cases (90.5%) than females (68.1%), with an odds ratio of 4.4 (95% CI, 2.17 to 9.62; *P* = 0.00004). The finding was bilateral in 14 of the animals (7%).

Intravitreal HRS. In 326 of 768 eyes (42.4%), SD-OCT revealed distinct HRS in the vitreous (Figure 3). Most of these lesions were round to oval in appearance; some displayed comma-shaped tails or were tapered at one end. They ranged in size from 15 μm to 150 μm in diameter. Most HRS were intermediate in size, averaging 20 μm to 30 μm in diameter. Given the vast number of these dots and the number of scans examined, only some representative HRS was measured; otherwise, the assessment was solely semiquantitative and descriptive. Female macaques (*n* = 98; 51.0%) were affected slightly more often than males (*n* = 76; 39.6%), corresponding to an odds ratio of 1.6 (95% CI, 1.06 to 2.39; *P* = 0.031). In the majority of cases (152 of 174 affected animals, 88%), HRS were found in both eyes; HRS were unilateral in 14 female and 8 male macaques (12% overall). To illustrate this strong correlation between eyes: in females, finding HRS in the first eye examined increased the probability of the second eye being affected from 7% to 92%, that is a factor of 13. In males, finding the first eye affected increased the chance of the second eye showing HRS from 3.3% to 94%, that is, by a factor of 28. In one female macaque, the right eye was

Table 1. Retinal findings in cynomolgus macaques assessed by using scanning laser ophthalmoscopy and optical coherence tomography

	Incidence (no. of animals/no. of eyes)	Female	Male	
Bergmeister papilla	184/198 (but scans of only 232 animals/464 eyes included the papilla)	79 (but scans from only 116 females included the papilla)	105 (but scans from only 116 males included the papilla)	Figure 2
	79.3 (73.5, 84.3)/42.6 (38.1, 47.3)	68.1 (58.8, 76.4)	90.5 (83.7, 95.2)	
Intravitreal hyperreflective spots	174/326	98	76	Figure 3
	45.3 (40.3, 50.4)/42.4 (38.9, 46.0)	51.0 (43.7, 58.3)	39.6 (32.6, 46.9)	
Tortuosity of retinal vasculature	2/4	0	2	Figure 4
	0.5 (0.1, 1.9)/0.5 (0.1, 1.3)			
Abnormally shaped foveal pit	6/12	4	2	Figure 5
	1.6 (0.6, 3.4)/1.6 (0.8, 2.7)			
Partial posterior vitreous detachment	1/1	0	1	Figure 6
	0.3 (<0.1, 1.4)/0.1 (<0.1, 0.7)			
Focal discontinuation of retinal layer(s)	4/4	0	4	Figure 7
	1.0 (0.3, 2.6)/0.5 (0.1, 1.3)			
Focal disorganization of retinal layers	1/1	0	1 (right eye)	Figure 8
	0.3 (<0.1, 1.4)/0.1 (<0.1, 0.7)			
Drusen-like subretinal hyperreflectivities	1/1	0	1 (right eye)	Figure 9
	0.3 (<0.1, 1.4)/0.1 (<0.1, 0.7)			
Vitreal opacity	1/1	0	1 (left eye)	Figure 4
	0.3 [<0.1, 1.4]/0.1 [<0.1, 0.7]			

Total no. of animals evaluated, 384; total no. of eyes evaluated, 768.
Data are given as case count (*n*) and incidence (%) and 95% CI (in parentheses).
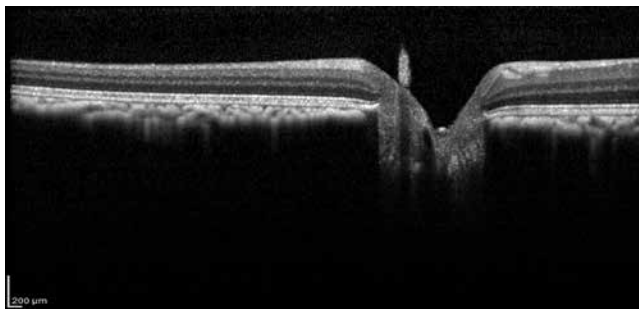

Figure 2. Bergmeister papilla. Note the conical structure extending from the papilla into the vitreous.
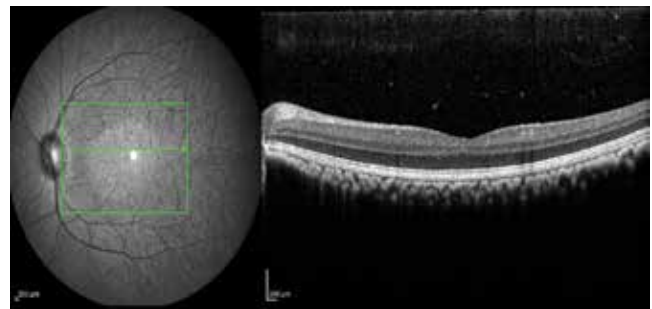

Figure 3. Intravitreal hyperreflectivities. Distinct hyperreflective whitish dots af variable size can be distinguished in the vitreous.

markedly more affected than the contralateral eye. In the rest of the animals with bilateral HRS, both eyes were comparable in regard to extent. Although their appearance in some eyes was confined to the peripapillary or parafoveal vitreous, HRS also occurred more peripherally in some eyes. Overall, HRS were distributed sparsely and evenly, in close proximity to the retinal surface.

Retinal vessel tortuosity. Two male macaques showed pronounced bilateral retinal vessel tortuosity on the SLO image (Figure 4). Tortuosity was present in all retinal arteries but not in the retinal veins. Tortuosity was marked in both eyes of one animal and moderate in both eyes of the other subject.

Unusually shaped foveal pit. All subjects included in the study had well-defined and similar foveal pits. However, 6 animals were remarkable because of bilaterally symmetrical, significantly larger and broader foveal pits compared with those in the remaining animals (Figure 5).

Partial posterior vitreous detachment. One eye showed localized posterior vitreous detachment next to the fovea (Figure 6). Below the posterior hyaloid, diffuse low-reflective material was detected.

Focal discontinuation of retinal layers. Four male macaques showed a small, unilateral focal discontinuation of the ellipsoid zone. In one of those eyes, underlying structures showed diffuse hyperreflectivity (Figure 7).

Figure 4. Tortuous retinal arteries.

Focal disorganization of retinal layering. Unilateral peripapillary disorganization of the retinal layers was found in a single male macaque (Figure 8).

Drusen-like subretinal hyperreflective deposits. Multifocal subretinal accumulations of hyperreflective material were noted unilaterally in the right eye of a single male animal. Corresponding coalescent hyperreflectivities were present on the autofluorescence fundus image (Figure 9).

Vitreal opacities. Unilateral opacity of the vitreous was present in the left eye of one male animal; this animal also had

unusually broad foveal pits (Figure 5). This finding presented as a shadow on the SLO image, whereas the vitreous depicted in the OCT scan lacked abnormal features.

Discussion

To our knowledge, this report is the first to describe the morphology and incidence of retinal OCT findings in cynomolgus monkeys. Hyperreflective spots occurred more frequently in female animals, and male macaques were affected with Bergmeister papillae more often than females. Otherwise, no appreciable sex-associated differences were noted. Several reports described the nature and frequency of such findings as noted on histopathology.[24,26,32] However, the findings affecting the vitreous, retina, and choroid—and therefore matching the regions assessed in the current study with OCT—vary in regard to pathologies described to the current study. Whereas some studies report no background findings in those ocular regions at all, others note disarrangement of retinal structures including folds, (cystoid) degeneration of the retina, nuclear displacement of the retina, conus of the optic nerve, glial nodules, or macular degeneration.[5,12,23,32]

Commonly observed were point-shaped foci, marked as intravitreal hyperreflective spots HRS. Of note, intravitreal HRS are not considered normal in the human population, but their presence has been reported in the context of ocular inflammatory diseases, after complicated posterior hyaloid detachments, and in the context of traumatic etiology and is thought to represent intravitreal cellular infiltrates or blood cells.[32] In the present study, concurrent ocular examinations with slit lamp and indirect biomicroscopy revealed no indication of associated inflammatory changes, and no signs of ocular trauma were observed. These foci could, therefore, be seen in the context of hyaloid artery remnants and its connective tissue called Bergmeister papilla. In humans, the hyaloid vasculature network regresses gradually beginning in the 4th month of gestation, and
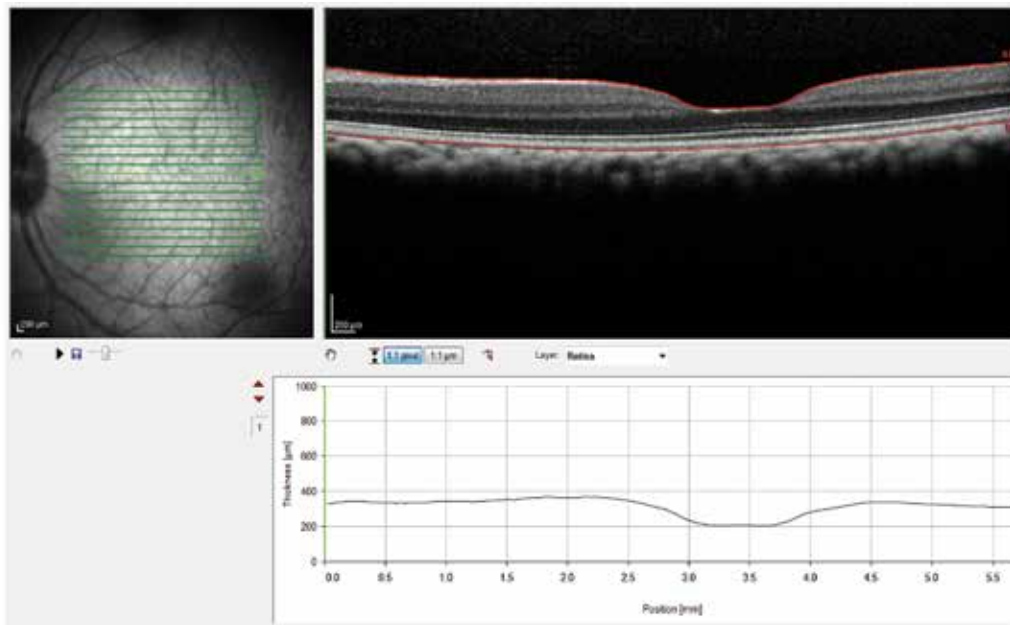

Figure 5. Abnormally shaped (flat) foveal pit (right) and vitreal opacity represented by the diffusely dark circular area in the lower right corner of the SLO image (left).
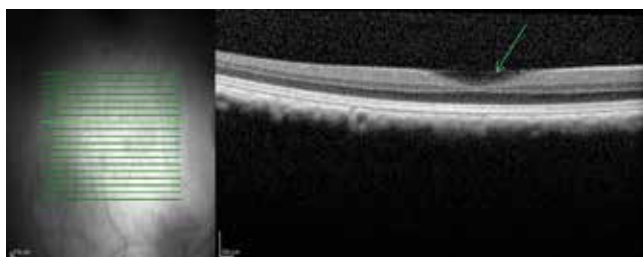
Figure 6. Partial posterior hyaloid detachment. The posterior hyaloid is detached in the fovea with diffuse low-reflective subhyaloidal material (green arrow).
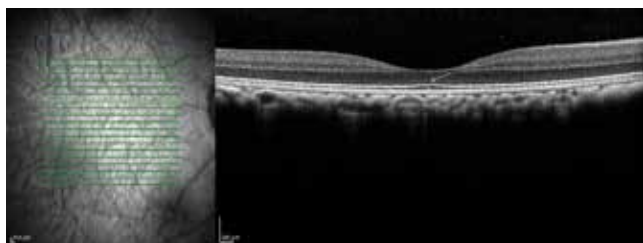

Figure 7. Focal interruption ellipsoid zone (green arrow in OCT image; right).

regression normally is complete by birth.[22] In NHP, considerable variability in regard to timing of complete disappearance has been reported.[10] In humans, the incidence of persistence of Bergmeister papilla and associated Cloquet canal were noted in 93%[14] and74%[25] respectively of eyes when examined with OCT; however, the sample size of those studies was limited. Notably, persistent fetal vasculature including Bergmeister papilla is most frequently unilateral in humans.[20] We observed the same pattern in the current study in cynomolgus monkeys. Given the frequency of affected eyes, there should be a much larger number of animals with bilateral findings (number expected, 42; number observed, 14). This result suggests that having one eye affected reduces the probability of the other eye being affected by a factor of 4.5.

Our frequent finding of persistent Bergmeister papilla in more than half of the eyes examined demonstrates that the remnant of the hyaloid artery and its associated structures do not regress completely in many eyes of cynomolgus monkeys. One also needs to take into account that the papilla was not depicted on the scans of all eyes examined; therefore, the true prevalence might exceed that frequency. Persistence of Bergmeister papilla can, therefore, be considered as an anatomic variant rather than an abnormal finding in this species. It could be speculated that both the high incidence of Bergmeister papilla and the earlier mentioned intravitreal HRS of potential vascular origin are linked, even though both findings could also be noted separately from the other in several eyes.

Further investigations are needed to characterize and identify the origin of these findings regarding HRS. In the meantime, awareness of this frequent background finding that shows intriguing similarity to inflammatory toxic pathologies will aid in discernment. Comparison of predose scans with longitudinally obtained scans throughout the study time course is needed to differentiate primary (background) findings from secondary findings relating to dosing or test article. However, it is important to note that the extent of intravitreal HRS varied greatly between different scans of the same eye

depending on the scan location and according to the mobility of the vitreous.

The fovea is the most important structure in the retina, responsible for the highest spatial acuity and color vision. Its characteristic displacement of the inner retina is thought to facilitate visual acuity, by decreasing light scatter.[30,31] Because of the specialized nature of the fovea, assessing its shape is potentially important when examining alterations associated with aging or disease.[7,15] In the current study, we performed a semiquantitative assessment only, which showed variations—namely a bilateral, broader foveal pit—in only a subset of macaques. In humans, ethnicity regarding the pigmentation of the ocular structures has been reported to directly influence the foveal width and depth, which are significantly narrower and shallower in the Caucasian population than in the black population.[6] Given the close genetic affinity of the cynomolgus macaques examined here, the observed deviations are likely to have a different cause, which still needs to be elucidated. Future studies are needed for a more detailed assessment of foveal curvature and symmetry, using a specialized OCT imaging protocol, as has already been done in humans.[29]

Our study population included 2 monkeys (0.5%) with bilateral arterial vessel tortuosity. Retinal vessel tortuosity is a common finding associated secondary to ocular inflammation and ischemic retinal disorders.[17] In these macaques, predominantly venous retinal vessels showed dilatation and tortuosity. Isolated arterial retinal vessel tortuosity, like that in our current study, is a rare finding in humans and has been reported to be inherited, as familial retinal arteriolar tortuosity.[28] The significance of retinal artery tortuosity remains unclear. Nevertheless, any vascular abnormalities of similar appearance are important to note during baseline examination, and inclusion of respective animals in a study or at least allocation to a particular dose group should be reconsidered depending on the readout parameters.

Identification of changes in the retinal architecture—such as disintegration of reflective bands, disorganization of layers, and drusen-like subretinal hyperreflectivities—on predose scans allows them to be differentiated from toxicologic changes during the study. Although most drusen classically are located beneath the retinal pigment epithelium, subretinal accumulation of drusen-like material has been reported in humans and variously termed pseudodrusen or subretinal drusenoid deposits.[16] A number of systemic diseases are associated with pseudodrusen, which are found more prevalent in the elderly human population. The fact that pseudodrusen was found in only a single eye of our study population may be attributable to the young age of those animals.

The vitreous body is an extracellular matrix that is relatively acellular. Vitreous consists of 98% water and macromolecules organized in a clear hyaluronic gel.[3,21] Changes in the vitreous filaments most often are a result of aging but also can originate from inflammation, vitreoretinal dystrophies, or myopic and diabetic vitreopathy.[19] The affected animal in the current study was young, and no other pathologies were detectable; therefore we can only speculate about the underlying etiology.

The findings in the present study and those described in other reports provided by the respective contract research organizations varied greatly among different studies and reviewers, ranging from 1% to 100%. Retinal findings were more likely to be reported than vitreous findings. Considering the importance of the vitreous in retinal disease, vitreal OCT findings reported in preclinical studies reports are surprisingly sparse. Whereas histologic assessment of the vitreous is limited given the challenges to focus on this structure, which consists primarily of
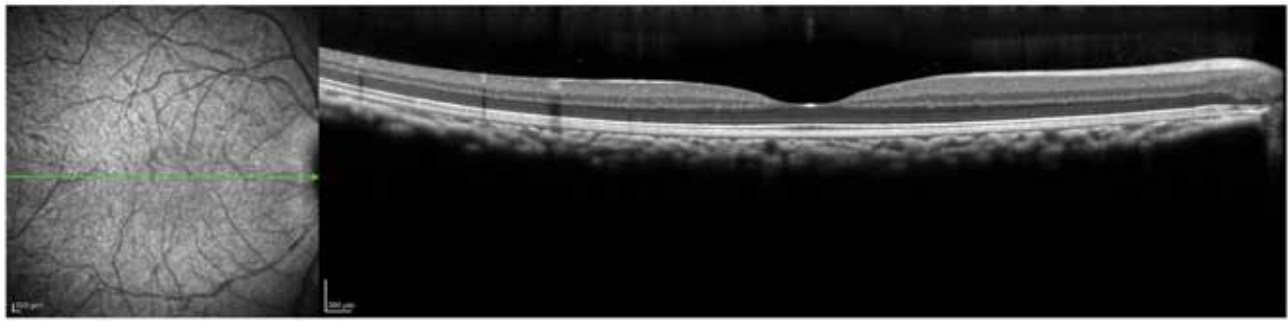
149

Figure 8. Peripapillary disturbance of retina layers and architecture. Note the loss of clear retinal layering in the peripapillary region (right side of the OCT image, left to the papilla; right).
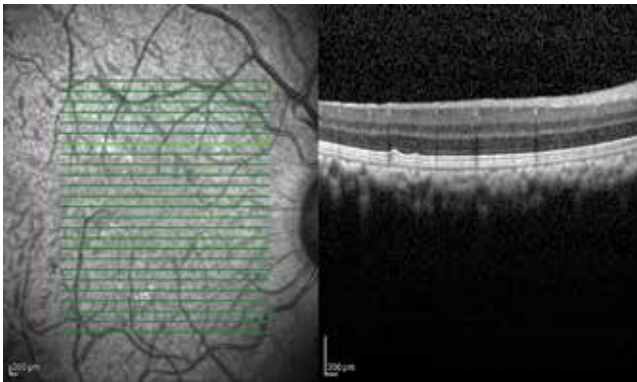

Figure 9. Drusenoid structures. Note the focal arching of the outer retinal layers.

water, OCT allows imaging of intraocular structures with increasing resolution, sensitivity, and depth.[6] Although the focus of preclinical OCT scans often lies on the retinal structures, the preretinal vitreous band (as a minimum) should not be neglected when reviewing the data set. Future refinement of the means for imaging vitreal structures is an important step to better understanding the potential effect of changes in the vitreous and vitreoretinal interface in the context of drug development studies.

Correlation of findings observed with OCT and histopathology is possible for selected pathologies,[9] often resulting in a description of OCT as "in-life histology."[18] OCT offers the tremendous benefit of noninvasive longitudinal imaging during the study, with a resolution exceeding other in vivo imaging techniques being used, and the image acquisition technique differs greatly from histology. Histologic examination allows a much higher resolution compared with OCT; however, OCT allows scans and images to be obtained faster and can be repeated as required, thus supporting screening and monitoring of larger regions of the eye. Furthermore, tissue assessed by histopathology has undergone several processing steps that, in turn, can influence parameters, such as thickness, of various structures. Histologic assessment of globes is often limited to one to three 4-µm sections for practical reasons, whereas with OCT, large numbers of scans per eye per imaging time point can readily be obtained, thus spanning a much larger proportion of the eye.

This benefit of in vivo and repeated imaging offered by OCT is strikingly reflected in the differences between findings of the current study and the reports describing the histologic background findings mentioned earlier. Although some pathologies, such as retinal disorganization or degeneration, may present similarly and correlate with each other on histology and OCT,

more attention should be paid to findings that are detectable only in vivo but not post mortem. Further refinement and standardization of ocular imaging in the preclinical setting will maximize the full potential of OCT imaging in this setting.

References

1. **Anger EM, Unterhuber A, Hermann B, Sattmann H, Schubert C, Morgan JE, Cowey A, Ahnelt PK, Drexler W.** 2004. Ultrahigh resolution optical coherence tomography of the monkey fovea. Identification of retinal sublayers by correlation with semithin histology sections. Exp Eye Res **78:**1117–1125. https://doi.org/10.1016/j.exer.2004.01.011.

2. **Atzpodien EA, Jacobsen B, Funk J, Altmann B, Silva Munoz MA, Singer T, Gyger C, Hasler P, Maloca P.** 2016. Advanced clinical imaging and tissue-based biomarkers of the eye for toxicology studies in minipigs. Toxicol Pathol **44:**398–413. https://doi.org/10.1177/0192623315615553.

3. **Bishop PN.** 2000. Structural macromolecules and supramolecular organisation of the vitreous gel. Prog Retin Eye Res **19:**323–344. https://doi.org/10.1016/S1350-9462(99)00016-6.

4. **Carpenter CL, Kim AY, Kashani AH.** 2018. Normative retinal thicknesses in common animal models of eye disease using spectral domain optical coherence tomography. Adv Exp Med Biol **1074:**157–166. https://doi.org/10.1007/978-3-319-75402-4_20.

5. **Chamanza R, Marxfeld HA, Blanco AI, Naylor SW, Bradley AE.** 2009. Incidences and range of spontaneous findings in control cynomolgus monkeys (*Macaca fascicularis*) used in toxicity studies. Toxicol Pathol **38:**642–657. https://doi.org/10.1177/0192623310368981.

6. **Ctori I, Huntjens B.** 2016. Variations in normative foveal morphology SD – OCT data: A study of White, South Asian and Black ethnicities. Abstracts from the 2016 European Association for Vision and Eye Research Conference, Nice, France, 5–8 October 2016. Acta Ophthalmol **94:**S256. https://doi.org/10.1111/j.1755-3768.2016.0527

7. **Elsner AE, Burns SA, Beausencourt E, Weiter JJ.** 1998. Foveal cone photopigment distribution: small alterations associated with macular pigment distribution. Invest Ophthalmol Vis Sci **39:**2394–2404.

8. **Fujimoto J, Huang D.** 2016. Foreword: 25 years of optical coherence tomography. Invest Ophthalmol Vis Sci **57:** OCTi–OCTii. https://doi.org/10.1167/iovs.16-20269.

9. **Ghazi NG, Dibernardo C, Ying H, Mori K, Gehlbach PL.** 2006. Optical coherence tomography of peripheral retinal lesions in enucleated human eye specimens with histologic correlation. Am J Ophthalmol **141:**740–742. https://doi.org/10.1016/j.ajo.2005.10.058.

10. **Hamming NA, Apple DJ, Gieser DK, Vygantas CM.** 1977. Ultrastructure of the hyaloid vasculature in primates. Invest Ophthalmol Vis Sci **16:**408–415.

11. **Huang D, Swanson EA, Lin CP, Schuman JS, Stinson WG, Chang W, Hee MR, Flotte T, Gregory K, Puliafito CA, Fujimoto JG.** 1991. Optical coherence tomography. Science **254:**1178–1181. https://doi.org/10.1126/science.1957169.

12. **Ito T, Chatani F, Sasaki S, Ando T, Miyajima H.** 1992. Spontaneous lesions in cynomolgus monkeys used in toxicity studies. Jikken Dobutsu **41:**455–469.

13. **Jindal A, Ctori I, Fidalgo B, Dabasia P, Balaskas K, Lawrenson JG**. 2019. Impact of optical coherence tomography on diagnostic decision-making by UK community optometrists: a clinical vignette study. Ophthalmic Physiol Opt **39:**205–215. https://doi.org/10.1111/opo.12613.

14. **Kagemann L, Wollstein G, Ishikawa H, Gabriele ML, Srinivasan VJ, Wojtkowski M, Duker JS, Fujimoto JG, Schuman JS.** 2006. Persistence of Cloquet's canal in normal healthy eyes. Am J Ophthalmol **142:**862–864. https://doi.org/10.1016/j.ajo.2006.05.059.

15. **Kanis MJ, Wisse RP, Berendschot TT, van de Kraats J, van Norren D.** 2008. Foveal cone-photoreceptor integrity in aging macula disorder. Invest Ophthalmol Vis Sci **49:**2077–2081. https://doi.org/10.1167/iovs.07-1181.

16. **Khan KN, Mahroo OA, Khan RS, Mohamed MD, McKibbin M, Bird A, Michaelides M, Tufail A, Moore AT.** 2016. Differentiating drusen: Drusen and drusen-like appearances associated with ageing, age-related macular degeneration, inherited eye disease and other pathological processes. Prog Retin Eye Res **53:**70–106. https://doi.org/10.1016/j.preteyeres.2016.04.008.

17. **Lee H, Lee M, Chung H, Kim HC.** 2018. Quantification of retinal vessel tortuosity in diabetic retinopathy using optical coherence tomography angiography. Retina **38:**976–985. https://doi.org/10.1097/IAE.0000000000001618.

18. **McLellan GJ, Rasmussen CA.** 2012. Optical coherence tomography for the evaluation of retinal and optic nerve morphology in animal subjects: practical considerations. Vet Ophthalmol **15 Suppl 2:**13–28. https://doi.org/10.1111/j.1463-5224.2012.01045.x.

19. **Milston R, Madigan MC, Sebag J.** 2016. Vitreous floaters: Etiology, diagnostics, and management. Surv Ophthalmol **61:**211–227. https://doi.org/10.1016/j.survophthal.2015.11.008.

20. **Nelson LB.** 2011. Pediatric ophthalmology: Color atlas and synopsis of clinical ophthalmology, 1st ed. Philadelphia (PA): Lippincott Williams and Wilkins.

21. **Reardon AJ, Le Goff M, Briggs MD, McLeod D, Sheehan JK, Thornton DJ, Bishop PN.** 2000. Identification in vitreous and molecular cloning of opticin, a novel member of the family of leucine-rich repeat proteins of the extracellular matrix. J Biol Chem **275:**2123–2129. https://doi.org/10.1074/jbc.275.3.2123.

22. **Saint-Geniez M, D'Amore PA.** 2004. Development and pathology of the hyaloid, choroidal and retinal vasculature. Int J Dev Biol **48:**1045–1058. https://doi.org/10.1387/ijdb.041895ms.

23. **Sato J, Doi T, Kanno T, Wako Y, Tsuchitani M, Narama I.** 2012. Histopathology of incidental findings in cynomolgus monkeys (*Macaca fascicularis*) used in toxicity studies. J Toxicol Pathol **25:**63–101. https://doi.org/10.1293/tox.25.63.

24. **Schuh JCL.** 2018. Letter to the Editor Regarding "Spontaneous Findings in the Eyes of Cynomolgus Monkeys (Macaca fascicularis) of Mauritian Origin" by Woicke et al. (Toxicol Pathol 46, 273–282, 2018). Toxicol Pathol **46:**719–720. https://doi.org/10.1177/0192623318791524.

25. **Sherman J, Nath S, Sadun A, Wong V, Delgado A, Boneta J, He W.** 2008. Spectral OCT Reveals Bergmeister's papillae in the majority of normal, young patients. ARVO Annual Meeting. Fort Lauderdale, Florida, April 27–01 May 2008. Invest Ophthalmol Vis Sci **49:**929.

26. **Sinha DP, Cartwright ME, Johnson RC.** 2006. Incidental mononuclear cell infiltrate in the uvea of cynomolgus monkeys. Toxicol Pathol **34:**148–151. https://doi.org/10.1080/01926230500531779.

27. **Staurenghi G, Sadda S, Chakravarthy U, Spaide RF; International Nomenclature for Optical Coherence Tomography (IN•OCT).** 2014. Proposed lexicon for anatomic landmarks in normal posterior segment spectral-domain optical coherence tomography: the IN*OCT consensus. Ophthalmology **121:**1572–1578. https://doi.org/10.1016/j.ophtha.2014.02.023.

28. **Sutter FK, Helbig H.** 2003. Familial retinal arteriolar tortuosity: a review. Surv Ophthalmol **48:**245–255. https://doi.org/10.1016/S0039-6257(03)00029-8.

29. **VanNasdale DA, Eilerman A, Zimmerman A, Lai N, Ramsey K, Sinnott LT.** 2017. Foveal curvature and asymmetry assessed using optical coherence tomography. Optom Vis Sci **94:**664–671. https://doi.org/10.1097/OPX.0000000000001084.

30. **Walls GL.** 1937. Significance of the foveal depression. Arch Ophthalmol **18:**912–919. https://doi.org/10.1001/archopht.1937.00850120046005.

31. **Williams DR.** 1980. Visual consequences of the foveal pit. Invest Ophthalmol Vis Sci **19:**653–667.

32. **Woicke J, Haile S, Mysore J, Peden WM, Lejeune T, Sanderson T, Brodie T.** 2018. Spontaneous findings in the eyes of cynomolgus monkeys (*Macaca fascicularis*) of Mauritian origin. Toxicol Pathol **46:**273–282. https://doi.org/10.1177/0192623318758619.